

Article

Energy Level Engineering of Donor Polymers via Inductive and Resonance Effects for Polymer Solar Cells: Effects of Cyano and Alkoxy Substituents

Heung Gyu Kim, Min Kim, J. Arul Clement, Jaewon Lee,
Jisoo Shin, Hyeongjin Hwang, Dong Hun Sin, and Kilwon Cho

Chem. Mater., **Just Accepted Manuscript** • DOI: 10.1021/acs.chemmater.5b03256 • Publication Date (Web): 25 Sep 2015

Downloaded from <http://pubs.acs.org> on September 26, 2015

Just Accepted

“Just Accepted” manuscripts have been peer-reviewed and accepted for publication. They are posted online prior to technical editing, formatting for publication and author proofing. The American Chemical Society provides “Just Accepted” as a free service to the research community to expedite the dissemination of scientific material as soon as possible after acceptance. “Just Accepted” manuscripts appear in full in PDF format accompanied by an HTML abstract. “Just Accepted” manuscripts have been fully peer reviewed, but should not be considered the official version of record. They are accessible to all readers and citable by the Digital Object Identifier (DOI®). “Just Accepted” is an optional service offered to authors. Therefore, the “Just Accepted” Web site may not include all articles that will be published in the journal. After a manuscript is technically edited and formatted, it will be removed from the “Just Accepted” Web site and published as an ASAP article. Note that technical editing may introduce minor changes to the manuscript text and/or graphics which could affect content, and all legal disclaimers and ethical guidelines that apply to the journal pertain. ACS cannot be held responsible for errors or consequences arising from the use of information contained in these “Just Accepted” manuscripts.

Energy Level Engineering of Donor Polymers via Inductive and Resonance Effects for Polymer Solar Cells: Effects of Cyano and Alkoxy Substituents

Heung Gyu Kim,[†] Min Kim,[†] J. Arul Clement,[†] Jaewon Lee, Jisoo Shin, Hyeongjin Hwang, Dong Hun Sin, and Kilwon Cho*

Department of Chemical Engineering
Pohang University of Science and Technology
Pohang 790-784, Korea
Email: kwcho@postech.ac.kr

[†] The authors contributed equally to this work.

Abstract

Fine tuning the energy levels of donor polymers is a critically important step toward achieving high power conversion efficiencies in polymer solar cells (PSCs). We systematically controlled the energy levels of donor polymers by introducing cyano (CN) and alkoxy (OR) groups into the 4,4'-didodecyl-2,2'-bithiophene (BT) unit in a step-by-step fashion, thereby varying the inductive and resonance effects. The three monomer units (BT, BTC, and BTCox) were polymerized with benzo[1,2-b:4,5-b']dithiophene (BDT) as a counter unit to afford three polymers (PBDT-BT, PBDT-BTC, and PBDT-BTCox). The highest occupied molecular orbital and lowest unoccupied molecular orbital energy levels decreased significantly upon the introduction of CN groups, and these levels increased slightly upon attachment of the OR groups, in good agreement with the measured open-circuit voltages of the three polymer devices. The strong inductive and resonance effects present in PBDT-BTCox narrowed the polymer band gap to 1.74 eV to afford a power conversion efficiency of 5.06%, the highest value achieved among the three polymers.

Introduction

Polymer solar cells (PSCs) have attracted wide interest as possible candidates for realizing lightweight flexible energy sources using low-cost large-area solution processes.¹⁻³ Until recently, bulk heterojunction (BHJ)-based PSCs prepared from blends of conjugated donor polymers and an acceptor, [6,6]-phenyl-C₆₁-butyric acid methyl ester (PC₆₁BM) or [6,6]-phenyl-C₇₁-butyric acid methyl ester (PC₇₁BM), have yielded the best enhancements in the power conversion efficiencies (PCEs).^{4,5} Donor polymers with a narrow band gap and a deep highest occupied molecular orbital (HOMO) energy level are needed to enhance light absorption and achieve a high short-circuit current density (J_{sc}) and high open circuit voltage (V_{oc}) because V_{oc} is strongly related to the difference between the HOMO energy level of the donor material and the lowest unoccupied molecular orbital (LUMO) energy level of the acceptor. Therefore, fine-tuning the band gap and energy level of the donor polymer is critically important for achieving a high PCE.⁶ To this end, three synthetic strategies have been developed to engineer the band gaps and control the energy levels of the donor polymers: (1) alternating donor-acceptor (D-A) structures, (2) aromaticity and bond length alternation in a polymer backbone (quinoid polymer), and (3) implementation of the inductive and resonance effects.⁷ Among these strategies, the alternating D-A concept, in which electron-rich (donor) and electron-deficient (acceptor) units are combined, has thus far been most widely applied and examined in donor polymers. This concept enables the facile tuning of the band gap, absorption spectrum, and energy levels of a donor polymer by varying the donor and acceptor units. Tremendous research efforts have been devoted to this strategy and exceptional advances have been achieved, with high PCEs of up to 10%.⁸⁻¹⁴

Quinoid polymers present another strategy for controlling the energy levels and band gaps. For instance, poly (thiophene) exhibits a relatively large band gap of 2.0 eV, whereas poly (benzo[c]thiophene), which includes a benzene ring bound to a thiophene ring, provides an

1
2
3
4 exceedingly small band gap of 1.0 eV due to the resonance energy of the benzene ring.^{15,16}
5
6 Recently, the PTB7-Th quinoid polymer has been tested in PSCs, providing a high PCE
7
8 (>10%) with a narrow band gap (1.59 eV).^{17,18}
9

10
11 Finally, inductive and resonance effects may be tuned by incorporating electron-donating
12
13 or electron-withdrawing substituents directly into the aromatic units of the main conjugated
14
15 polymer backbone. The inductive and resonance effects are effective in adjusting the energy
16
17 levels and band gaps in the donor polymer. In general, electron-donating groups increase the
18
19 HOMO energy level, whereas electron-withdrawing groups reduce the LUMO energy level.¹⁹
20
21 For instance, the cyano (CN) group is a typical electron-withdrawing group and can lower
22
23 both the HOMO and the LUMO energy levels with respect to the corresponding levels of the
24
25 analogues prepared without the CN groups.²⁰⁻²³ Alternatively, the HOMO energy level may
26
27 be increased and the band gap narrowed upon the introduction of an alkoxy (OR) electron-
28
29 donating group to the backbone of the conjugated polymer.²⁴ Therefore, the energy level and
30
31 band gap of a donor polymer may be finely tuned by modulating the inductive and resonance
32
33 effects. Synthetic strategy of mainly utilizing inductive and resonance effects has not yet been
34
35 extensively studied for donor polymers in PSCs despite the recognized effectiveness of
36
37 inductive and resonance strategies for energy level control.
38
39
40

41
42 This work primarily focused on the systematic study of inductive and resonance effects in
43
44 an effort to engineer the energy levels and band gaps of donor polymers. To this end, three
45
46 monomer units were designed and synthesized by successively introducing CN and OR
47
48 groups onto the 4,4'-didodecyl-2,2'-bithiophene (BT) unit. The BT moiety was used as a
49
50 reference structure. First, we introduced CN groups as electron-withdrawing groups into the
51
52 BT unit to synthesize the 4,4'-didodecyl-3,3'-dicyano-2,2'-bithiophene (BTC) unit. Second, an
53
54 OR electron-donating group was introduced into the BTC unit to synthesize 4,4'-
55
56 didodecyloxy-3,3'-dicyano-2,2'-bithiophene (BTCox). These monomer units were
57
58
59
60

1
2
3
4 polymerized with benzo[1,2-b:4,5-b']dithiophene (BDT) as a counter unit to afford three
5
6 polymers (PBDT-BT, PBDT-BTC, and PBDT-BTCox). The PBDT-BT reference polymer
7
8 consisted only of donor units without any acceptor moieties, to exclude D–A alternating
9
10 effects. We then investigated the effects of the CN and OR groups on the energy level, band
11
12 gap, and device performance in detail. The HOMO energy level was dramatically lowered
13
14 from -5.37 eV to -5.58 eV upon introduction of a CN group, and the band gap narrowed
15
16 significantly from 2.1 eV to 1.74 eV upon introduction of both CN and OR groups due to
17
18 inductive and resonance effects. Moreover the crystallinity of the polymers changed
19
20 considerably upon introduction of the substituents. PBDT-BTCox yielded the highest
21
22 crystallinity because the CN and OR groups formed a strong resonance structure, and the S–O
23
24 non-covalent interactions in the polymer backbone enhanced the planarity of the polymer
25
26 backbone. The best PCE, 5.06% , was achieved in the PBDT-BTCox-based single-junction
27
28 device under AM 1.5G illumination. We demonstrated that the inductive and resonance
29
30 effects offered a powerful synthetic strategy for fine-tuning the energy levels and band gaps
31
32 of the conjugated polymers.
33
34
35
36
37
38
39

40 **Results and Discussion**

41 **Synthesis of Monomers and Polymers**

42
43
44 The general synthetic route to the monomers is described in Scheme 1. The BDT
45
46 monomer was synthesized according to the procedure reported in the literature.²⁵ 4-Dodecyl-
47
48 3-cyanothiophene (5) and 4-dodecyloxy-3-cyanothiophene (8) were synthesized according to
49
50 methods described previously and were coupled to afford the BTC monomer (6) and BTCox
51
52 monomer (10).^{21,26} As described in Scheme 2, a Stille coupling polymerization between the
53
54 BDT monomer and three monomers (BT, BTC, and BTCox) gave three new polymers
55
56 (PBDT-BT, PBDT-BTC, and PBDT-BTCox) after standard purification. The synthesized
57
58
59
60

1
2
3
4 polymers were soluble in chlorinated solvents, such as chlorobenzene (CB), o-
5 dichlorobenzene (o-DCB), and chloroform. The number-average molecular weights (M_n) and
6 polydispersity indices (PDIs) of the polymers were evaluated by gel permeation
7 chromatography (GPC) at 40 °C using CB as the eluent. The M_n values of PBDT-BT, PBDT-
8 BTC, and PBDT-BTCox were 14.8, 11.8, and 37.6 kDa, with PDIs of 1.93, 3.37, and 1.77,
9 respectively. The polymers exhibited good thermal stability with a decomposition
10 temperature (T_d) exceeding 390 °C, determined using thermogravimetric analysis (TGA), as
11 shown in Figure S1 and Table 1. The thermotropic properties of the polymers were
12 characterized by differential scanning calorimetry (DSC). DSC measurements did not reveal
13 any endothermic or exothermic behavior between 30 °C and 250 °C. Although there is a
14 slight deviance of PDIs and M_n of the synthesized polymers, these differences might not
15 largely change intrinsic polymer properties such as absorption, energy level, crystallinity and
16 DFT calculation according to previous reports.²⁷⁻²⁹

32 33 34 35 **Optical Properties**

36
37 The UV-visible absorption spectra of the polymers were obtained in chloroform solutions
38 and in thin films, as shown in Figure 1a. The absorption spectra gradually red-shifted with the
39 introduction of CN (PBDT-BTC) and OR groups (PBDT-BTCox). The maximum absorption
40 wavelengths (λ_{max}) of PBDT-BT, PBDT-BTC, and PBDT-BTCox, measured in solution,
41 were at 468, 448, and 629 nm, respectively, whereas the corresponding values measured in
42 the thin films were 518, 529, and 635 nm. The absorption spectra of the polymers were red-
43 shifted in the thin films due to the increased π - π interchain interactions upon aggregation. The
44 optical band gaps (E_g^{opt}) of PBDT-BT, PBDT-BTC, and PBDT-BTCox were calculated from
45 the absorption edges in the thin films and were found to be 2.10, 1.96, and 1.74 eV,
46 respectively. The PBDT-BT reference polymer exhibited a large band gap of 2.10 eV, as

1
2
3
4 expected. The PBDT-BTC polymer prepared with CN groups yielded a band gap that was
5
6 slightly reduced, to 1.96 eV, because the CN groups slightly stabilized the quinoid structure
7
8 of the BT unit via the inductive and resonance effects of the CN groups. The band gap of the
9
10 PBDT-BTCox polymer, prepared with CN and OR groups, decreased significantly to 1.74 eV
11
12 because the quinoid structure throughout the polymer backbone was strongly stabilized by the
13
14 inductive and resonance effects of the CN and OR groups. The measured λ_{\max} and E_g^{opt}
15
16 values are listed in Table 1. Moreover the effects of the optical absorption were investigated
17
18 by measuring the absorption coefficients (α) of the polymers. PBDT-BTCox displayed the
19
20 highest maximum among the polymers, an α of 635 nm, which was twice the value of α for
21
22 PBDT-BTC (Figure S2).
23
24
25
26
27

28 **Resonance Structures**

29
30 The influence of the substituents on the electronic structure of the polymer may be
31
32 described in terms of two effects: the inductive and resonance effects. The inductive effect
33
34 involves the transmission of electrostatic charge through the σ -bonds, mediated by the
35
36 electronegativity of the atoms, whereas the resonance effect involves the transmission of
37
38 electron density through the π -system of the molecules via the electron-donating or -
39
40 withdrawing properties of the substituents, as described using the relevant resonance
41
42 structures. Figure 2 shows the resonance structures of the respective monomer moieties. In
43
44 the reference structure comprising the BT unit with alkyl groups, the carbon atom was
45
46 slightly more electronegative than the hydrogen atom in the alkyl chain. The small dipole
47
48 moment of this structure pulled electron density away from hydrogen and toward the carbon
49
50 in the alkyl chain. The slight buildup of electron density on the carbon in the alkyl group
51
52 induced a small degree of electron donation via the inductive effect (+I). The CN groups on
53
54 the BTC unit withdrew electron density through inductive (-I) and resonance (-R) effects.
55
56
57
58
59
60

1
2
3
4 The quinoid structure of the BTC unit was more stabilized than the BT unit as a result of the
5 inductive and resonance effects of the CN groups. The oxygen atom on the BTCox unit
6 bearing OR and CN groups was more electronegative than the carbon atom, and the electron
7 density was withdrawn as a result of the inductive effect (–I). Simultaneously, the lone pair
8 electrons of the oxygen atom could be donated back into the thiophene ring through
9 resonance effect (+R). In this case, the resonance effect (+R) of the OR groups was more
10 powerful than the inductive effect (–I). The quinoid structure of the BTC unit was strongly
11 stabilized by both the resonance effect (+R) of the OR groups and the resonance effect (–R)
12 of the CN groups.
13
14
15
16
17
18
19
20
21
22
23
24
25

26 **Electrochemical Properties**

27
28 The electrochemical properties of the synthesized polymers were investigated using
29 cyclic voltammetry (CV), as shown in Figure S3. The HOMO/LUMO energy levels of
30 PBDT-BT, PBDT-BTC, and PBDT-BTCox were calculated to be –5.37/–3.25, –5.58/–3.53,
31 and –5.50/–3.51 eV, with ferrocene as a reference (Table 1 and Figure 1b). PBDT-BTC and
32 PBDT-BTCox exhibited deep HOMO energy levels (<–5.5 eV) upon the addition of the CN
33 groups, thereby ensuring good air stability and a high V_{oc} in PSC applications. PBDT-BTC
34 with PBDT-BT were compared, revealing that the HOMO energy level of PBDT-BTC
35 dramatically decreased, from –5.37 to –5.58 eV, and the LUMO energy level also decreased,
36 from –3.25 to –3.53 eV, as a result of the inductive (–I) and resonance effects (–R) of the CN
37 groups. The band gap (E_g^{cv}) decreased slightly, from 2.12 to 2.05 eV, due to the inductive (–
38 I) and resonance effects (–R) of the CN groups. The PBDT-BTCox polymer bearing OR and
39 CN groups yielded a HOMO energy level that slightly increased, from –5.58 to –5.50 eV, due
40 to the resonance effect (+R) of the OR groups. In particular, PBDT-BTCox displayed both
41
42
43
44
45
46
47
48
49
50
51
52
53
54
55
56
57
58
59
60

1
2
3
4 inductive and resonance effects in the thiophene units, thereby dramatically reducing the
5
6 band gap (E_g^{cv}) to 1.99 eV due to the strong stabilization of the quinoid structure.
7

8
9
10 Molecular simulations of the polymers were performed using density functional theory
11 (DFT) calculation at the B3LYP/6-31G* level to investigate the effects of the CN and OR
12 groups. The alkyl groups in the structures were replaced with methyl groups that do not
13 significantly affect the equilibrium geometries or electronic properties of the molecules. The
14
15 calculated HOMO and LUMO levels were found to agree well with the energy levels
16
17 measured using CV. Although DFT calculations usually provide higher values than CV
18
19 measurements, both methods revealed similar trends in the energy levels. The
20
21 HOMO/LUMO energy levels of PBDT-BT were found to be $-4.74/-2.22$ eV. A comparison
22
23 of PBDT-BTC with PBDT-BT revealed that the LUMO energy level decreased dramatically
24
25 from -2.22 to -2.92 eV, and the HOMO energy level also decreased from -4.74 to -5.35 eV
26
27 as a result of the inductive ($-I$) and resonance effects ($-R$) of CN groups. A comparison of
28
29 PBDT-BTCox with PBDT-BTC revealed that the LUMO energy level decreased from -2.92
30
31 to -3.10 eV whereas the HOMO energy level increased from -5.35 to -5.22 eV due to the
32
33 strong resonance effect ($+R$) of the OR groups. The resulting theoretical (DFT) and
34
35 experimental (CV) HOMO and LUMO levels agreed well, as illustrated in Figure 1b.
36
37
38
39
40
41

42 We further examined the structural properties of the polymers. Two dihedral angles, the
43
44 first between the BDT unit and the thiophene unit (θ_1) and the second between the two
45
46 thiophene units (θ_2) in the polymers, were calculated, as shown in Figure 3. The θ_1 and θ_2
47
48 values obtained from PBDT-BT were calculated to be 19.54° and 13.42° . The dihedral
49
50 angles of PBDT-BTC (θ_1 : 30.35° , θ_2 : 19.72°) became more twisted upon introduction of the
51
52 CN groups into the BT moiety due to the increased steric hindrance relative to the hindrance
53
54 introduced by hydrogen atoms. Interestingly, the dihedral angles (θ_1 : 6.71° , θ_2 : 0.29°) of
55
56
57
58
59
60

PBDT-BTCox were incredibly reduced due to the strong stabilization of the quinoid structure of the polymer backbone via the inductive and resonance effects of both the CN and OR groups and the effects of S-O non-covalent interactions (inter-locking).³⁰⁻³² These results indicate that introducing substituents could considerably change the planarity of the polymer backbone in addition to changing the energy levels.

X-ray Diffraction Properties

Grazing incidence X-ray diffraction (GIXD) measurements were collected to investigate the crystalline properties of the polymers.³³⁻³⁶ The GIXD patterns obtained from the three neat polymer films revealed distinct structural differences, as shown in Figure 4. The out-of-plane (OOP) GIXD profile of the neat PBDT-BT film displayed pronounced lamellar stacking (h00) peaks at 0.31 \AA^{-1} and 0.62 \AA^{-1} arising from the alkyl chain packing, with a d-spacing of 20 \AA . The in-plane (IP) profile of the neat PBDT-BT film showed a weak (100) peak at 0.31 \AA^{-1} and a strong π - π stacking (010) peak at 1.54 \AA^{-1} , which corresponded to (010) π - π stacking with a d-spacing of 4.08 \AA . These results suggested that the neat PBDT-BT film was formed predominantly with an edge-on molecular orientation with respect to the substrate. The OOP profiles collected from the neat PBDT-BTC film showed weak lamellar stacking (h00) peaks at 0.29 \AA^{-1} and a pronounced π - π stacking (010) peak at 1.54 \AA^{-1} . The IP profile revealed a stronger (100) peak in the OOP profile, indicating that a face-on molecular orientation dominated the neat PBDT-BTC film. By comparison, the GIXD profiles of the neat PBDT-BTCox film showed prominent (h00) and (010) peaks in both the OOP and IP profiles, suggesting that the PBDT-BTCox polymer assumed a bimodal orientation distribution containing both edge-on and face-on orientations. The GIXD patterns obtained from the neat PBDT-BTC films revealed low-order and low-intensity lamellar stacking (h00) peaks compared to the corresponding peaks collected from the PBDT-BT

1
2
3
4 polymer. These results confirmed that the steric hindrance of the CN groups in the BT unit
5
6 disrupted molecular packing. On the other hand, the GIXD pattern of the neat PBDT-BTCox
7
8 polymer exhibited prominent higher-order (h00) diffraction peaks that were attributed to the
9
10 enhanced planarity of the polymers due to stabilization of the quinoid structure of the
11
12 polymer backbone and the effects of the S-O interaction, as fully supported by the DFT
13
14 molecular simulations and circularly integrated XRD profiles (Figure S5). Interestingly, the
15
16 molecular planarity and packing compactness of the polymers also reflected the π - π stacking
17
18 distance between polymer chains, revealing that the PBDT-BTCox molecules (3.80 Å) were
19
20 shorter than the PBDT-BT molecules (4.08 Å). The presence of the fullerene (in a blend film
21
22 comprising PC₇₁BM) did not fully disrupt the crystal structures of the polymer, and the
23
24 diffraction peak of PC₇₁BM was clearly observed. The crystal structure of the PBDT-BTCox
25
26 polymer was beneficial for charge transport in the photovoltaic devices because it assumed a
27
28 face-on orientation and a reduced π - π stacking distance between the polymer backbones.³⁷⁻³⁹
29
30
31
32
33
34

35 **Solar Cell Performance**

36
37 Polymer solar cells were fabricated using the three polymers as a donor material and
38
39 PC₇₁BM as an acceptor material. The device architecture was ITO/MoO₃/polymer:PC₇₁BM/
40
41 LiF/Al, and the device area was 0.055 cm². The MoO₃ layer was used as a hole transport
42
43 layer with a high work function that was energetically aligned to the deep HOMO energy
44
45 level (< -5.5 eV).^{40,41} The thickness and blend weight ratios of the polymer/PC₇₁BM film
46
47 were optimized, as listed in Table 2. The 1:2 weight blend ratio of the polymer/PC₇₁BM films
48
49 processed from o-DCB exhibited the best performance for all three polymers. The addition of
50
51 the solvent additive, 1,8-diiodooctane (DIO), enhanced the photovoltaic performances only in
52
53 the case of PBDT-BTCox and not in the cases of the PBDT-BT and PBDT-BTC polymers, as
54
55
56
57
58
59
60

1
2
3
4 explained by the atomic force microscopy (AFM) morphological characterization images
5
6 (Figure 6).
7

8
9 The current density versus voltage curves (J - V) collected under AM 1.5 conditions with
10 an intensity of 100 mW cm^{-2} are presented in Figure 5a, and the average device parameters
11 are listed in Table 2. Among the three polymer devices, the PBDT-BTCox device exhibited
12 the highest power conversion efficiency, with $V_{oc} = 0.86 \text{ V}$, $J_{sc} = 10.1 \text{ mA cm}^{-2}$, $\text{FF} = 58.4\%$,
13 and $\text{PCE} = 4.80\%$ ($\text{PCE}_{\text{max}} = 5.06\%$). The V_{oc} values of PBDT-BT (0.82 V), PBDT-BTC
14 (0.90 V), and PBDT-BTCox (0.86 V) exactly corresponded to the differences between the
15 measured HOMO energy levels of the three polymers (-5.37 eV , -5.58 eV , and -5.50 eV ,
16 respectively) and the LUMO energy levels of PC₇₁BM. The external quantum efficiencies
17 (EQEs) of these devices are shown in Figure 5b. The EQE spectra of the PBDT-BTC and
18 PBDT-BTCox devices were red-shifted (29 and 86 nm, respectively) compared to those of
19 the PBDT-BT device, in good agreement with the UV-Vis absorption results (Figure S7).
20 Despite the red-shifted absorption maximum of the PBDT-BTC device, the maximum of
21 EQE did not exceed 10% and resulted in a poor J_{sc} . This decrease relates to the largely phase-
22 separated morphology on a length scale of hundreds of nanometers, as illustrated in the AFM
23 images. On the other hand, the PBDT-BTCox device exhibited the highest EQE maximum
24 ($\sim 55\%$) and J_{sc} (10.1 mA cm^{-2}), with an absorption maximum that was red-shifted from 300
25 nm to 721 nm and agreed well with the UV-Vis spectrum.
26
27
28
29
30
31
32
33
34
35
36
37
38
39
40
41
42
43
44
45

46 Insight into the fill factors of the polymer/PC₇₁BM devices was sought by measuring the
47 charge transport properties using the space-charge-limited current (SCLC) method.⁴²⁻⁴⁵ The
48 results were fit to the model $J = (9/8)\epsilon\mu(V^2/L^3)$, where ϵ is the static dielectric constant of
49 the medium and μ is the carrier mobility, in hole-dominant devices with the structure
50 ITO/MoO₃/polymer: PC₇₁BM/MoO₃/Al.^{46,47} The fits to the J - V curve, based on the SCLC
51
52
53
54
55
56
57
58
59
60

1
2
3
4 model, are shown in Figure S4. The hole mobilities were calculated to be $3.34 \times 10^{-6} \text{ cm}^2 \text{ V}^{-1} \text{ s}^{-1}$
5
6 $1.23 \times 10^{-8} \text{ cm}^2 \text{ V}^{-1} \text{ s}^{-1}$ for PBDT-BT/PC₇₁BM, $1.23 \times 10^{-8} \text{ cm}^2 \text{ V}^{-1} \text{ s}^{-1}$ for PBDT-BTC/PC₇₁BM, and 5.64×10^{-5}
7
8 $\text{ cm}^2 \text{ V}^{-1} \text{ s}^{-1}$ for PBDT-BTCox/PC₇₁BM (weight ratio of the donor versus acceptor is 1:2),
9
10 respectively. The hole mobilities were closely related to the molecular structures and
11
12 crystallinities. The closely packed molecular structure of the PBDT-BTCox polymer
13
14 particularly contributed to the high hole mobility and fill factor (59%) of the PBDT-
15
16 BTCox/PC₇₁BM device compared to the corresponding values measured from the PBDT-BT
17
18 (46%) and PBDT-BTC (41%) devices. The differences in hole mobilities of the three
19
20 polymers agreed with the crystallinities of the polymers, as measured using GIXD.
21
22
23

24 AFM images were collected to assess the morphological structures of the
25
26 polymer/PC₇₁BM blend films. The PBDT-BT/PC₇₁BM blend film assumed a phase-separated
27
28 morphology on the ~100 nm length scale (Figure 6a). This morphology was not beneficial for
29
30 the BHJ structure due to the limited exciton diffusion length, on the ~10 nm length scale.^{48,49}
31
32 The AFM image obtained from the PBDT-BTC/PC₇₁BM blend film also revealed significant
33
34 phase separation, with PC₇₁BM aggregates about ~200 nm in length (Figure 6b). This
35
36 morphology clearly explained the low J_{sc} value measured from the PBDT-BTC device.
37
38 Unfortunately, the morphologies of the PBDT-BT and PBDT-BTC blend films changed
39
40 slightly when processed with DIO (Figure 6d, 6e). The addition of DIO did not improve the
41
42 photovoltaic performances of the PBDT-BT and PBDT-BTC devices. On the contrary, the
43
44 PBDT-BTCox/PC₇₁BM blend film revealed a nanoscale intermixed morphology in the well-
45
46 developed BHJ structure (Figure 6c). When processed with DIO, the PBDT-BTCox blend
47
48 morphology also revealed nanoscale phase separation that improved the efficiency of charge
49
50 separation (Figure 6f). The morphological differences among the polymer:PC₇₁BM blend
51
52 films could be explained by comparing the measured surface energies of the polymers and
53
54 PC₇₁BM.⁵⁰ We confirmed that the observed severe phase separation in the PBDT-
55
56
57
58
59
60

1
2
3
4 BT:PC₇₁BM and PBDT-BTC:PC₇₁BM blend films corresponded to the large differences
5 among the surface energies of the polymer and fullerene (PBDT-BT: 21.78 mN m⁻¹, PBDT-
6 BTC: 16.51 mN m⁻¹, PC₇₁BM: 23.66 mN m⁻¹). PBDT-BTCox displayed a surface energy
7 (22.51 mN m⁻¹) similar to that measured in PC₇₁BM, consistent with the observed nano-scale
8 separated morphology (Figure S6).
9
10
11
12
13
14
15
16

17 **Conclusions**

18
19 We systematically studied the energy levels and band gaps of the donor polymers in
20 which the inductive and resonance effects had been tuned through synthetic engineering.
21 Three monomer units were designed and synthesized by introducing the CN and OR groups
22 onto the BT unit in a step-by-step manner. The synthesized monomers were polymerized with
23 the BDT unit as a counter monomer to afford three polymers (PBDT-BT, PBDT-BTC, and
24 PBDT-BTCox). We investigated the effects of the CN and OR groups on the energy level,
25 band gap, and device performance. The HOMO energy level decreased dramatically, from –
26 5.37 to –5.58 eV, upon the introduction of CN groups, and the band gap (E_g^{opt}) narrowed
27 significantly, from 2.1 to 1.74 eV, upon introduction of both CN and OR groups via the strong
28 inductive and resonance effects. The resultant photovoltaic performances were characterized
29 by high open-circuit voltages (V_{oc}) ranging from 0.82 V to 0.98 V. In the polymer series, the
30 polymer solar cell based on a blend of PBDT-BTCox and PC₇₁BM gave the best photovoltaic
31 performance, with a V_{oc} of 0.86 V and a PCE of 5.06%. We demonstrated that synthetically
32 tuning the inductive and resonance effects provided a powerful strategy for fine-tuning the
33 energy levels and band gaps of the donor polymers.
34
35
36
37
38
39
40
41
42
43
44
45
46
47
48
49
50
51
52
53
54

55 **Experimental Section**

56 **Materials**

1
2
3
4 All reagents were purchased from Aldrich, TCI and Acros, and used without further
5 purification. All anhydrous organic solvents for synthesis and device fabrication such as
6 tetrahydrofuran (THF), chloroform, toluene, N, N-dimethylformamide (DMF), chlorobenzene
7 (CB), o-dichlorobenzene (o-DCB) were purchased from Aldrich. The compounds, 5,5'-
8 dibromo-4,4'-didodecyl-2,2'-bithiophene, 3-cyano-4-dodecylthiophene, and BDT monomer
9 were synthesized according to literature procedures.^{21,24,25}
10
11
12
13
14
15
16

17 **Characterization**

18
19 ¹H and ¹³C NMR spectra were recorded on a Bruker AVANCE 400 operating at 400 MHz
20 and 100 MHz respectively in chloroform-d solutions with tetramethylsilane (TMS) as the
21 internal standard. Number-average (M_n) and weight-average (M_w) molecular weights were
22 measured by gel permeation chromatography (GPC) using a Shimadzu LC solution with CB
23 as the eluent and a calibration curve of polystyrene standards at 40 °C. UV-vis absorption
24 spectra were obtained with a Varian CARY 5000 UV/Visible Spectrophotometer. Differential
25 scanning calorimetry (DSC) and thermogravimetric analysis (TGA) were performed by using
26 a DSC 2910 (TA Instruments) and a TGA 2050 (TA Instruments) under a nitrogen
27 atmosphere at a heating and cooling rate of 10 °C min⁻¹. Cyclic voltammograms were
28 recorded using a PowerLab/AD Instruments model system. A 0.1 M tetrabutylammonium
29 hexafluorophosphate (Bu₄NPF₆) solution in acetonitrile was used as the electrolyte solution.
30 The three electrode system consisted of an Ag/AgCl reference electrode, a glassy carbon
31 working electrode, and a platinum counter electrode. Polymer thin films were prepared by
32 drop casting polymer solutions in chloroform onto the working electrode. The potential of the
33 Ag/AgCl reference electrode was internally calibrated by using the ferrocene/ferrocenium
34 redox couple (Fc/Fc⁺). The energy levels were estimated with the equations: $E_{\text{HOMO}} = -(4.80$
35 $+ E_{\text{onset, ox}})$, and $E_{\text{LUMO}} = -(4.80 + E_{\text{onset, red}})$. The film morphologies were characterized with
36
37
38
39
40
41
42
43
44
45
46
47
48
49
50
51
52
53
54
55
56
57
58
59
60

1
2
3
4 atomic force microscopy (AFM, Digital Instruments Multimode). The thicknesses of the
5
6 polymer films were measured by using an ellipsometer (M-2000V, J. A. Woollam Co., Inc.).
7
8 2D grazing incidence X-ray diffraction grazing incidence X-ray diffraction (GIXD) was
9
10 performed by using the synchrotron source at the Pohang Accelerator Laboratory (PAL) in
11
12 Korea. 2D GIXD patterns were recorded with a 2D CCD detector (Rayonix SX165) and the
13
14 X-ray irradiation time was 1 ~ 10 s depending on the saturation level of the detector.
15
16

17 **Computational details**

18
19 Density functional theory (DFT) calculations were performed using the Gaussian 09
20
21 package with the nonlocal hybrid Becke three-parameter Lee-Yang-Parr (B3LYP) function
22
23 and the 6-31G* basis set after optimizing the geometry of oligomers.
24
25

26 **Monomer synthesis**

27
28 **2-Bromo-3-dodecylthiophene 1.** 3-dodecylthiophene (5 g, 19.8 mmol) was added to a dry
29
30 chloroform (30 mL) and acetic acid (30 mL) solution. NBS (3.53 g, 19.8 mmol) was added
31
32 slowly and then stirred for 2 h at room temperature. After addition of water (50 mL), organic
33
34 phase was separated and extracted with chloroform (2 × 20 mL). The combined extracts were
35
36 dried over anhydrous MgSO₄, filtered and distillation of solvent under reduced pressure. The
37
38 oily residue was purified by column chromatography using hexane as the eluent to afford 5.4
39
40 g of compound 1 (82% yield) as a colorless oily liquid. ¹H NMR (400 MHz, CDCl₃, ppm) δ:
41
42 7.19 (d, 1H, J = 5.6 Hz), 6.81 (d, 1H, J = 5.6 Hz), 2.58 (t, 2H, J = 7.8 Hz), 1.58 (m, 2H, J =
43
44 7.5 Hz), 1.36-1.30 (m, 18H), 0.91 (t, 3H, J = 7.0 Hz). ¹³C NMR (100 MHz, CDCl₃, ppm) δ:
45
46 141.9, 128.2, 125.1, 108.8, 31.9, 29.8, 29.7, 29.6, 29.5, 29.4, 29.3, 29.2, 22.7, 14.1.
47
48
49

50
51 **5,5'-Dibromo-4,4'-didodecyl-2,2'-bithiophene 2.** The mixture of a
52
53 Bis(benzonitrile)palladium (II) chloride (0.09 g, 0.24 mmol), 20 mL of DMSO, and 2-bromo-
54
55 3-dodecylthiophene (5 g, 15.09 mmol) was stirred. To the resulting mixture, silver (I)
56
57 fluoride (3.82 g, 2 equiv) was added and heated at 60 °C for 12 h. Then, the mixture was
58
59
60

1
2
3
4 cooled to room temperature and passed through a Celite pad, which was successively washed
5
6 with chloroform. The filtrate was washed with water and the combined organic layer was
7
8 dried over anhydrous MgSO_4 and concentrated under reduced pressure. The crude residue
9
10 was purified by column chromatography using hexane as the eluent. Recrystallization of
11
12 crude product using dichloromethane and methanol gave 3.9 g of compound 2 (78% yield) as
13
14 a yellow solid. ^1H NMR (400 MHz, CDCl_3 , ppm) δ : 6.79 (s, 2H), 2.52 (t, 4H, $J = 7.8$ Hz),
15
16 1.56 (m, 4H, $J = 7.3$ Hz), 1.34-1.28 (m, 36H), 0.89 (t, 6H, $J = 7.0$ Hz). ^{13}C NMR (100 MHz,
17
18 CDCl_3 , ppm) δ : 142.9, 136.1, 124.4, 107.8, 31.9, 29.7, 29.6, 29.5, 29.4, 29.3, 29.2, 22.7, 14.1.

19
20
21 **2,3,5-Tribromo-4-dodecylthiophene 3.** Bromine (5.12 mL, 100 mol) was added dropwise
22
23 over a period of 1.5 h to a solution of 3-dodecylthiophene (8 g, 31.68 mmol) in anhydrous
24
25 chloroform (50 mL) in the presence of a catalytic amount of Fe powder. The reaction mixture
26
27 was stirred for 2 h. After careful addition of water (50 mL), the mixture was slowly
28
29 neutralized by an aqueous solution of 2M NaOH (40 mL). The aqueous phase was extracted
30
31 with dichloromethane (2×50 mL). The organic layer was collected and washed with a
32
33 saturated aqueous solution of $\text{Na}_2\text{S}_2\text{O}_3$, dried over MgSO_4 , and concentrated under reduced
34
35 pressure. The crude residue was purified by column chromatography using hexane as the
36
37 eluent to afford 13.8 g of compound 3 (89 % yield) as an orange oil. ^1H NMR (400 MHz,
38
39 CDCl_3 , ppm) δ : 2.68 (t, 2H, $J = 7.8$ Hz), 1.58 (m, 2H, $J = 7.5$ Hz), 1.36-1.30 (m, 18H), 0.91 (t,
40
41 3H, $J = 7.0$ Hz). ^{13}C NMR (100 MHz, CDCl_3 , ppm) δ : 141.7, 118.2, 109.1, 108.8, 31.9, 29.8,
42
43 29.7, 29.6, 29.5, 29.4, 29.3, 29.2, 22.7, 14.1.

44
45
46
47
48 **3-Bromo-4-dodecylthiophene 4.** n-BuLi (2.5M in hexane, 21.3 mL, 53.25 mmol) was
49
50 slowly added over a period of 2 h to a solution of 2,3,5-tribromo-4-dodecylthiophene (13 g,
51
52 26.57 mmol) in anhydrous Et_2O (100 mL) cooled to -5 °C. After 20 min of additional stirring
53
54 at -5 °C, the reaction mixture was carefully hydrolyzed at -5 °C with vigorous stirring by
55
56 addition of an aqueous solution of 4M HCl (20 mL). The mixture was diluted with Et_2O (50
57
58
59
60

mL) and slowly warmed to room temperature. The aqueous phase was separated and extracted with Et₂O (2 × 50 mL). The organic phase was separated and washed with water (2 × 150 mL), dried over MgSO₄, and evaporated. The oily residue was purified by column chromatography on silica gel using hexane as the eluent to afford 8.1 g of compound 4 (92 % yield) as a slightly yellow oil. ¹H NMR (400 MHz, CDCl₃, ppm) δ: 7.24 (d, 1H, J = 3.5 Hz), 6.98 (d, 1H, J = 3.4 Hz), 2.60 (t, 2H, J = 7.5 Hz), 1.58 (m, 2H, J = 7.5 Hz), 1.36-1.31 (m, 18 H), 0.91 (t, 3H, J = 7.02 Hz). ¹³C NMR (100 MHz, CDCl₃, ppm) δ: 128.3, 122.6, 120.5, 112.7, 31.9, 29.9, 29.7, 29.4, 29.3, 29.2, 22.7, 14.1.

4-Dodecyl-3-cyanothiophene 5. A mixture of 3-Bromo-4-dodecylthiophene (8 g, 24.1 mmol) and CuCN (2.5 g, 27.9 mmol) in anhydrous DMF (50 mL) was refluxed for 38 h. The reaction mixture was cooled to 60 °C before a solution of FeCl₃ (7.8 g, 48.3 mmol) in an aqueous solution of 8M HCl (40 mL) was added. The mixture was then cooled to room temperature and extracted with dichloromethane. The organic layer was washed with water, dried over MgSO₄, and evaporated under reduced pressure. The oily residue was purified by column chromatography on silica gel using dichloromethane and hexane (1:4) to afford 6.4 g of compound 5 (95 % yield) as an orange oil. ¹H NMR (400 MHz, CDCl₃, ppm) δ: 7.86 (d, 1H, J = 3.3 Hz), 7.01 (d, 1H, J = 3.2 Hz), 2.75 (t, 2H, J = 7.7 Hz), 1.63 (m, 2H), 1.41–1.31 (m, 18 H), 0.90 (t, 3H, J = 7.01 Hz). ¹³C NMR (100 MHz, CDCl₃, ppm) δ: 145.5, 134.4, 122.8, 116.1, 112.9, 31.8, 29.7, 29.4, 29.2, 29.1, 29.0, 22.6, 14.1

5,5'-Dibromo-4,4'-didodecyl-3,3'-dicyano-2,2'-bithiophene 6. To a dry chloroform solution (25 mL) containing 4-dodecyl-3-cyanothiophene (1 g, 3.61 mmol), catalytic amount of Fe powder was added. Bromine (0.63 g, 3.97 mmol) was added slowly and then stirred for 12 h at room temperature. Organic phase was separated and extracted with chloroform (2 × 20 mL). The combined extracts were dried over anhydrous MgSO₄, filtered and distillation of solvent under reduced pressure. The crude product was used next step without further

1
2
3
4 purification. The mixture of a Bis(benzonitrile)palladium (II) chloride (0.03 g, 0.08 mmol),
5
6 20 mL of DMSO, and 5-bromo-4-dodecylthiophene-3-carbonitrile (1 g, 2.80 mmol) was
7
8 stirred. To the resulting mixture, silver (I) fluoride (0.70 g, 2 equiv) was added and heated at
9
10 60 °C for 12 h. Then, the mixture was cooled to room temperature and passed through a
11
12 Celite pad, which was successively washed with chloroform. The filtrate was washed with
13
14 water and the aqueous layer was extracted with chloroform (3 × 50 mL). The combined
15
16 organic layer was dried over MgSO₄ and concentrated under reduced pressure to give a crude
17
18 solid. The crude solid was purified by column chromatography on silica gel using
19
20 dichloromethane and hexane (1:2) as the eluent. Recrystallization of the product using
21
22 dichloromethane and methanol gave 0.4 g of compound 6 (40% yield) as a yellow solid. ¹H
23
24 NMR (400 MHz, CDCl₃, ppm) δ: 2.36 (t, 4H, J = 7.4 Hz), 1.68-1.63 (m, 4H), 1.32-1.27 (m,
25
26 36H), 0.90 (t, 6H, J = 6.8 Hz). ¹³C NMR (100 MHz, CDCl₃, ppm) δ: 144.8, 140.3, 113.6,
27
28 112.8, 110.8, 31.9, 29.6, 29.4, 29.3, 29.2, 29.1, 22.7, 14.1. Elemental analysis: calc. for
29
30 C₃₄H₅₀Br₂N₂S₂: C, 57.46; H, 7.09; N, 3.94; S 9.02. Found: C, 57.54; H, 7.03; N, 3.86; S,
31
32 9.08%.

33
34
35
36
37 ***4-Dodecyloxy-3-cyano-2,5-dihydrothiophene*** 7. To a solution of 3-cyano-4-
38
39 oxotetrahydrothiophene (2 g, 15.73 mmol) in 15 mL of DMF, Cs₂CO₃ (6.14 g, 1.2 equiv) and
40
41 dodecyl methanesulfonate (5 g, 1.2 equiv) were added. The solution was irradiated in CEM
42
43 microwave oven (T = 80 °C) for 10 min. After the completion of the reaction, the mixture
44
45 was poured into water, and extracted with dichloromethane (3 × 50 mL). The combined
46
47 organic layer was washed several times with water and dried with MgSO₄. After evaporation
48
49 of the solvent, the residue was purified through column chromatography using hexane and
50
51 ethyl acetate (10:1) as the eluent to afford 3.4 g of compound 7 (73% yield) as a pale yellow
52
53 oily liquid. ¹H NMR (400 MHz, CDCl₃, ppm) δ: 4.30 (t, 2H, J = 6.4 Hz), 3.76 (s, 4H), 1.74-
54
55
56
57
58
59
60

1
2
3
4 1.67 (m, 2H), 1.29-1.23 (m, 18H), 0.86 (t, 3H, J = 6.8 Hz). ¹³C NMR (100 MHz, CDCl₃, ppm)
5
6 δ: 168.9, 115.7, 80.6, 72.3, 36.0, 34.1, 31.9, 29.6, 29.5, 29.4, 29.3, 29.2, 25.6, 22.7, 14.1.

7
8 **4-Dodecyloxy-3-cyanothiophene 8.** A solution of 4-dodecyloxy-3-cyano-2,5-
9 dihydrothiophene (3 g 10.15 mmol) in dichloromethane (50 mL) was stirred at 50 °C then a
10 solution of DDQ (2.77 g, 1.2 equiv) in THF (20 mL) was slowly added. After addition, the
11 reaction mixture was stirred for 12 h. After addition of water (100 mL), the mixture was
12 extracted with dichloromethane (3 × 50 mL). The organic phase was dried over MgSO₄ and
13 evaporated under reduced pressure. The resulting oil was purified by column chromatography
14 on silica gel using hexane and ethyl acetate (10:1) as the eluent to afford 2.5 g of compound 8
15 (84% yield) as a colorless solid. ¹H NMR (400 MHz, CDCl₃, ppm) δ: 7.77 (s, 1H, ArH), 6.27
16 (s, 1H, ArH), 4.0 (t, 2H, J = 6.6 Hz), 1.86-1.79 (m, 2H), 1.48-1.43 (m, 2H), 1.28 (m, 16H),
17 0.89 (t, 3H, J = 6.8 Hz). ¹³C NMR (100 MHz, CDCl₃, ppm) δ: 157.6, 134.1, 113.4, 104.1, 97.9,
18 71.3, 31.9, 29.6, 29.5, 29.4, 29.3, 28.9, 25.9, 22.7, 14.1.

19
20
21
22
23
24
25
26
27
28
29
30
31
32
33 **5-Bromo-4-dodecyloxy-3-cyanothiophene 9.** NBS (1.82 g, 1.2 equiv) was slowly added
34 to a solution of 4-dodecyloxy-3-cyanothiophene (2.5 g, 8.51 mmol) in chloroform (30 mL).
35 The reaction mixture was heated at 50 °C for 10 h in dark. After addition of water (30 ml),
36 the mixture was extracted with dichloromethane (3 × 50 mL). The organic phase was dried
37 over MgSO₄ and evaporated under reduced pressure. The resulting oil was purified by
38 column chromatography on silica gel using hexane and ethyl acetate (10:1) as the eluent to
39 afford 2.9 g of compound 9 (91% yield) as a pale yellow liquid. ¹H NMR (400 MHz, CDCl₃,
40 ppm) δ: 7.79 (s, 1H, ArH), 4.24 (t, 2H, J = 6.6 Hz), 1.84-1.77 (m, 2H), 1.53-1.48 (m, 2H),
41 1.33- 1.28 (m, 16H), 0.896 (t, 3H, J = 6.8 Hz). ¹³C NMR (100 MHz, CDCl₃, ppm) δ: 154.5,
42 133.8, 112.9, 106.6, 98.2, 75.0, 31.9, 29.9, 29.7, 29.6, 29.5, 29.4, 29.3, 25.7, 22.7, 14.1.

43
44
45
46
47
48
49
50
51
52
53
54
55 **5,5'-Dibromo-4,4'-didodecyloxy-3,3'-dicyano-2,2'-bithiophene 10.** The mixture of a
56 Bis(benzonitrile)palladium (II) chloride (0.06 g, 0.16 mmol), 30 mL of DMSO, and 5-bromo-

1
2
3
4 4-dodecyloxy-3-cyanothiophene (2.9 g, 7.79 mmol) was stirred. To the resulting mixture,
5
6 silver (I) fluoride (2.17 g, 2.2 equiv) was added and heated at 60 °C for 7 h. Then, the
7
8 mixture was cooled to room temperature and passed through a Celite pad, which was
9
10 successively washed with chloroform. The filtrate was washed with water and extracted with
11
12 chloroform (3 × 50 mL). The combined organic layer was dried over MgSO₄ and
13
14 concentrated under reduced pressure to give a crude solid. The crude solid was purified by
15
16 column chromatography on silica gel using dichloromethane and hexane (1:2) as the eluent.
17
18 Recrystallization of the product using dichloromethane and methanol gave 1.6 g of
19
20 compound 10 (55% yield) as a yellow solid. ¹H NMR (400 MHz, CDCl₃, ppm) δ: 4.28 (t, 4H,
21
22 J = 6.6 Hz), 1.86-1.79 (m, 4H), 1.55-1.47 (m, 4H), 1.28 (m, 32H), 0.90 (t, 6H, J = 6.8 Hz).
23
24 ¹³C NMR (100 MHz, CDCl₃, ppm) δ: 155.4, 138.2, 112.3, 105.2, 100.3, 75.5, 31.9, 29.9, 29.7,
25
26 29.6, 29.5, 29.4, 29.3, 25.6, 22.7, 14.1. Elemental analysis: calc. for C₃₄H₅₀Br₂N₂O₂S₂: C,
27
28 54.98; H, 6.79; N, 3.77; S 8.63. Found: C, 54.88; H, 6.69; N, 3.78; S, 8.78%.

32 33 **Polymer synthesis**

34
35 **PBDT-BT.** Compound 2 (0.26 g, 0.39 mmol), BDT monomer (0.30 g, 0.39 mmol), and
36
37 Pd(PPh₃)₄ (9 mg) were dissolved in a mixture of toluene (13 mL) and DMF (1 mL). The
38
39 reaction flask was purged with nitrogen for 1 h. The solution was refluxed for 3 days at
40
41 120 °C, and then cooled to room temperature. The polymer solution was poured into
42
43 methanol (200 mL). The resulting solid was filtered and Soxhlet extracted with methanol,
44
45 acetone, hexane, and chloroform until the wash solution of each extraction was colorless. The
46
47 chloroform fraction was concentrated and poured into methanol, filtered, and dried under
48
49 vacuum to afford 0.26 g (72% yield) of red solid. ¹H NMR (400 MHz, CDCl₃), δ (ppm):
50
51 7.67-7.07 (m, 4H), 4.31-4.21 (br, 4H), 2.96-2.52 (br, 4H), 1.95-0.84 (br, 76H). GPC (CB,
52
53 40 °C): M_n = 14.85 kDa, M_w = 28.63 kDa, PDI = 1.93. Elemental analysis: calc. for
54
55 C₅₈H₈₈O₂S₄: C, 73.67; H, 9.38; S 13.56. Found: C, 73.26; H, 9.24; S, 13.83%.

1
2
3
4 **PBDT-BTC.** Compound 6 (0.184 g, 0.26 mmol) and BDT monomer (0.20 g, 0.26 mmol)
5
6 were used as the monomers. Yield: 0.17 g (66%). ^1H NMR (400 MHz, CDCl_3), δ (ppm):
7
8 7.72-6.94 (m, 2H), 4.32-4.16 (br, 4H), 3.14-2.97 (br, 4H), 1.94-0.75 (br, 76H). GPC (CB,
9
10 40 °C): $M_n = 11.82$ kDa, $M_w = 39.83$ kDa, PDI = 3.37. Elemental analysis: calc. for
11
12 $\text{C}_{60}\text{H}_{86}\text{N}_2\text{O}_2\text{S}_4$: C, 72.38; H, 8.71; N, 2.81; S 12.88. Found: C, 72.13; H, 8.48; N, 2.61; S,
13
14 13.02%.
15

16
17 **PBDT-BTCox.** Compound 10 (0.25 g, 0.337 mmol) and BDT monomer (0.26 g, 0.337
18
19 mmol) were used as the monomers. Yield: 0.31 g (89%). ^1H NMR (400 MHz, CDCl_3), δ
20
21 (ppm): 8.70-6.71 (m, 2H), 4.68-3.79 (br, 8H), 1.97-0.74 (br, 76H). GPC (CB, 40 °C): $M_n =$
22
23 37.59 kDa, $M_w = 66.73$ kDa, PDI = 1.77. Elemental analysis: calc. for $\text{C}_{60}\text{H}_{86}\text{N}_2\text{O}_4\text{S}_4$: C,
24
25 70.13; H, 8.44; N, 2.73; S 12.48. Found: C, 70.17; H, 8.24; N, 2.62; S, 12.59%.
26
27
28
29
30

31 **Fabrication and characterization of the polymer solar cells**

32
33 **OPV fabrication.** An ITO patterned glass ($15 \Omega \text{ sq}^{-1}$) was cleaned by sonication with warm
34
35 acetone and isopropyl alcohol followed by UV-ozone treatment. After ITO cleansing, 9 nm
36
37 MoO_3 film was formed by thermal evaporation of MoO_3 powder. PC_{71}BM (99.5%, Solenne,
38
39 Inc.) were used as acceptor materials in this study. The polymer: PC_{71}BM blend solutions
40
41 were prepared in 1,2-dichlorobenzene solution at 70 °C for 1 day. 1,8-diiodooctane (DIO)
42
43 was added into the solution (1.5 v%) and stirred for 20 minutes before spin-coating. The
44
45 DIO-added blend solutions were then spin-cast onto the MoO_3 coated ITO glasses and dried
46
47 for 1 h in N_2 environment, giving total thickness of 90~110 nm depending on optimum
48
49 thicknesses at respective conditions. The blend films were dried under high vacuum ($<10^{-6}$
50
51 Torr) for 12 hours to completely remove the residual solvent. On the tops of these films, 6 Å
52
53
54
55
56
57
58
59
60

1
2
3
4 of LiF and 120 nm of Al were formed by thermal evaporation as the cathode. The working
5
6 areas for devices were 0.055 cm².
7

8 **Electrical Characterization.** The current-voltage (*J-V*) characteristics were measured using
9
10 a Keithley 4200 power source under AM 1.5G illumination at an intensity of 100 mW cm⁻²
11
12 (Oriel 1 kW solar simulator) with PVM 132 reference cell certified by NREL. All electrical
13
14 measurements and fabrication processes were performed under inert N₂ environment. The
15
16 external quantum efficiency (EQE) was measured using a photomodulation spectroscopy
17
18 setup (Merlin, Oriel) with monochromatic light from a xenon lamp. The power density of the
19
20 monochromatic light was calibrated using a Si photodiode certified by the National Institute
21
22 for Standards and Technology (NIST).
23
24
25
26
27

28 **Supporting information**

29
30 Detail characterization of polymers (TGA, CV, absorption coefficient, XRD), SCLC, contact
31
32 angle, and normalized EQE curves. This information is available free of charge via the
33
34 Internet at <http://pubs.acs.org/>.
35
36
37
38

39 **Acknowledgements**

40
41 H. G. Kim, M. Kim, and J. Arul Clement contributed equally to this work. This work was
42
43 supported by a grant (Code No. 2011-0031628) from the Center for Advanced Soft
44
45 Electronics under the Global Frontier Research Program of the Ministry of Science, ICT and
46
47 Future Planning, Korea. The authors thank the Pohang Accelerator Laboratory for providing
48
49 the synchrotron radiation sources at 3C and 9A beam lines used in this study.
50
51
52
53
54
55
56
57
58
59
60

References

- (1) Günes, S.; Neugebauer, H.; Sariciftci, N. S. Conjugated Polymer-Based Organic Solar Cells. *Chem. Rev.* **2007**, *107*, 1324.
- (2) Thompson, B. C.; Fréchet, J. M. J. Polymer–Fullerene Composite Solar Cells. *Angew. Chem., Int. Ed.* **2008**, *47*, 58.
- (3) Brabec, C. J.; Sariciftci, N. S.; Hummelen, J. C. Plastic Solar Cells. *Adv. Funct. Mater.* **2001**, *11*, 15.
- (4) Park, J. H.; Kim, J. S.; Lee, J. H.; Lee, W. H.; Cho, K. Effect of Annealing Solvent Solubility on the Performance of Poly(3-hexylthiophene)/Methanofullerene Solar Cells. *J. Phys. Chem. C* **2009**, *113*, 17579.
- (5) Kim, J.-H.; Park, J. H.; Lee, J. H.; Kim, J. S.; Sim, M.; Shim, C.; Cho, K. Bulk Heterojunction Solar Cells Based on Preformed Polythiophene Nanowires via Solubility-Induced Crystallization. *J. Mater. Chem.* **2010**, *20*, 7398.
- (6) Zhou, H.; Yang, L.; You, W. Rational Design of High Performance Conjugated Polymers for Organic Solar Cells. *Macromolecules* **2012**, *45*, 607.
- (7) Cheng, Y.-J.; Yang, S.-H.; Hsu, C.-S. Synthesis of Conjugated Polymers for Organic Solar Cell Applications. *Chem. Rev.* **2009**, *109*, 5868.
- (8) Coffin, R. C.; Peet, J.; Rogers, J.; Bazan, G. C. Streamlined Microwave-Assisted Preparation of Narrow-Bandgap Conjugated Polymers for High Performance Bulk Heterojunction Solar Cells. *Nat. Chem.* **2009**, *1*, 657.
- (9) Zhang, Y.; Hau, S. K.; Yip, H.-L.; Sun, Y.; Acton, O.; Jen, A. K.-Y. Efficient Polymer Solar Cells Based on the Copolymers of Benzodithiophene and Thienopyrroledione. *Chem. Mater.* **2010**, *22*, 2696.
- (10) Zhou, N.; Guo, X.; Ortiz, R. P.; Li, S.; Zhang, S.; Chang, R. P. H.; Facchetti, A.; Marks, T. J. Bithiophene Imide and Benzodithiophene Copolymers for Efficient Inverted Polymer Solar Cells. *Adv. Mater.* **2012**, *24*, 2242.
- (11) Lee, J.; Jo, S. B.; Kim, M.; Kim, H. G.; Shin, J.; Kim, H.; Cho, K. Donor–Acceptor Alternating Copolymer Nanowires for Highly Efficient Organic Solar Cells. *Adv. Mater.* **2014**, *26*, 6706.
- (12) Nguyen, T. L.; Choi, H.; Ko, S.-J.; Uddin, M. A.; Walker, B.; Yum, S.; Jeong, J.-E.; Yun, M. H.; Shin, T. J.; Hwang, S.; Kim, J. Y.; Woo, H. Y. Semi-Crystalline Photovoltaic Polymers with Efficiency Exceeding 9% in a ~300 nm Thick Conventional Single-Cell Device. *Energy Environ. Sci.* **2014**, *7*, 3040.
- (13) Ho, C.-C.; Chen, C.-A.; Chang, C.-Y.; Darling, S. B.; Su, W.-F. Isoindigo-Based Copolymers for Polymer Solar Cells with Efficiency over 7%. *J. Mater. Chem. A* **2014**, *2*, 8026.

1
2
3
4 (14) Liu, Y.; Zhao, J.; Li, Z.; Mu, C.; Ma, W.; Hu, H.; Jiang, K.; Lin, H.; Ade, H.; Yan, H.
5 Aggregation and Morphology Control Enables Multiple Cases of High-Efficiency Polymer
6 Solar Cells. *Nat. Commun.* **2014**, *5*, 5293.
7

8 (15) Roncali, J. Molecular Engineering of the Band Gap π -Conjugated Systems: Facing
9 Technological Applications. *Macromol. Rapid Commun.* **2007**, *28*, 1761.
10

11 (16) Chen, H. Y.; Hou, J. H.; Zhang, S. Q.; Liang, Y. Y.; Yang, G. W.; Yang, Y.; Yu, L. P.;
12 Wu, Y.; Li, G. Polymer Solar Cells with Enhanced Open-Circuit Voltage and Efficiency. *Nat.*
13 *Photonics* **2009**, *3*, 649.
14

15 (17) He, Z.; Xiao, B.; Liu, F.; Wu, H.; Yang, Y.; Xiao, S.; Wang, C.; Russell, T. P.; Cao, Y.
16 Single-Junction Polymer Solar Cells with High Efficiency and Photovoltage. *Nat. Photonics*
17 **2015**, *9*, 174.
18

19 (18) Chen, J.-D.; Cui, C.; Li, Y.-Q.; Zhou, L.; Ou, Q.-D.; Li, C.; Li, Y.; Tang, J.-X. Single-
20 Junction Polymer Solar Cells Exceeding 10% Power Conversion Efficiency. *Adv. Mater.*
21 **2015**, *27*, 1035.
22

23 (19) Zhang, Q. T.; Tour, J. M. Alternating Donor/Acceptor Repeat Units in Polythiophenes.
24 Intramolecular Charge Transfer for Reducing Band Gaps in Fully Substituted Conjugated
25 Polymers. *J. Am. Chem. Soc.* **1998**, *120*, 5355.
26

27 (20) Thompson, B. C.; Kim, Y.-G.; McCarley, T. D.; Reynolds, J. R. Soluble Narrow Band
28 Gap and Blue Propylenedioxythiophene-Cyanovinylene Polymers as Multifunctional
29 Materials for Photovoltaic and Electrochromic Applications. *J. Am. Chem. Soc.* **2006**, *128*,
30 12714.
31

32 (21) Hergué, N.; Mallet, C.; Savitha, G.; Allain, M.; Frère, P.; Roncali, J. Facile Synthesis of
33 3-Alkoxy-4-cyanothiophenes as New Building Blocks for Donor-Acceptor Conjugated
34 Systems. *Org. Lett.* **2011**, *13*, 1762.
35

36 (22) Rudenko, A. E.; Khlyabich, P. P.; Thompson, B. C. Random Poly(3-hexylthiophene-*co*-
37 3-cyanothiophene) Copolymers via Direct Arylation Polymerization (DAP) for Organic
38 Solar Cells with High Open-Circuit Voltage. *ACS Macro Lett.* **2014**, *3*, 387.
39

40 (23) Casey, A.; Han, Y.; Fei, Z.; White, A. J. P.; Anthopoulos, T. D.; Heeney, M. Cyano
41 substituted benzothiadiazole: a novel acceptor inducing n-type behaviour in conjugated
42 polymers. *J. Mater. Chem. C* **2015**, *3*, 265.
43

44 (24) Huo, L.; Zhang, S.; Guo, X.; Xu, F.; Li, Y.; Hou, J. Replacing Alkoxy Groups with
45 Alkylthienyl Groups: A Feasible Approach to Improve the Properties of Photovoltaic
46 Polymers. *Angew. Chem., Int. Ed.* **2011**, *50*, 9697.
47

48 (25) Hou, J.; Park, M.-H.; Zhang, S.; Yao, Y.; Chen, L.-M.; Li, J.-H.; Yang, Y. Bandgap and
49 Molecular Energy Level Control of Conjugated Polymer Photovoltaic Materials Based on
50 Benzo[1,2-*b*:4,5-*b'*]dithiophene. *Macromolecules* **2008**, *41*, 6012.
51

- 1
2
3
4 (26) Blanchard, P.; Verlhac, P.; Michaux, L.; Frère, P.; Roncali, J. Fine Tuning of the
5 Electronic Properties of Linear π -Conjugated Oligomers by Covalent Bridging. *Chem. Eur. J.*
6 **2006**, *12*, 1244.
7
- 8 (27) Lee, H. K. H.; Li, Z.; Constantinou, I.; So, F.; Tsang, S. W.; So, S. K. Batch-to-Batch
9 Variation of Polymeric Photovoltaic Materials: its Origin and Impacts on Charge Carrier
10 Transport and Device Performances. *Adv. Energy Mater.* **2014**, *4*, 1400768.
11
- 12 (28) Liu, C.; Wang, K.; Hu, X.; Yang, Y.; Hsu, C.-H.; Zhang, W.; Xiao, S.; Gong, X.; Cao, Y.
13 Molecular Weight Effect on the Efficiency of Polymer Solar Cells. *ACS Appl. Mater.*
14 *Interfaces* **2013**, *5*, 12163.
15
- 16 (29) Bartelt, J. A.; Douglas, J. D.; Mateker, W. R.; Labban, A. E.; Tassone, C. J.; Toney, M.
17 F.; Fréchet, J. M. J.; Beaujuge, P. M.; McGehee, M. D. Controlling Solution-Phase Polymer
18 Aggregation with Molecular Weight and Solvent Additives to Optimize Polymer-Fullerene
19 Bulk Heterojunction Solar Cells. *Adv. Energy Mater.* **2014**, *4*, 1301733.
20
- 21 (30) Hwang, H.; Khim, D.; Yun, J.-M.; Jung, E.; Jang, S.-Y.; Jang, Y. H.; Noh, Y.-Y.; Kim,
22 D.-Y. Quinoidal Molecules as a New Class of Ambipolar Semiconductor Originating from
23 Amphoteric Redox Behavior. *Adv. Funct. Mater.* **2015**, *25*, 1146.
24
- 25 (31) Kim, H. G.; Kang, B.; Ko, H.; Lee, J.; Shin, J.; Cho, K. Synthetic Tailoring of Solid-State
26 Order in Diketopyrrolopyrrole-Based Copolymers via Intramolecular Noncovalent
27 Interactions. *Chem. Mater.* **2015**, *27*, 829.
28
- 29 (32) Jackson, N. E.; Savoie, B. M.; Kohlstedt, K. L.; de la Cruz, M. O.; Schatz, G. C.; Chen,
30 L. X.; Ratner, M. A. Controlling Conformations of Conjugated Polymers and Small
31 Molecules: The Role of Nonbonding Interactions. *J. Am. Chem. Soc.* **2013**, *135*, 10475.
32
- 33 (33) Baker, J. L.; Jimison, L. H.; Mannsfeld, S.; Volkman, S.; Yin, S.; Subramanian, V.;
34 Salleo, A.; Alivisatos, A. P.; Toney, M. F. Quantification of Thin Film Crystallographic
35 Orientation Using X-ray Diffraction with an Area Detector. *Langmuir* **2010**, *26*, 9146.
36
- 37 (34) Rivnay, J.; Mannsfeld, S. C. B.; Miller, C. E.; Salleo, A.; Toney, M. F. Quantitative
38 Determination of Organic Semiconductor Microstructure from the Molecular to Device Scale.
39 *Chem. Rev.* **2012**, *112*, 5488.
40
- 41 (35) Olivier, Y.; Niedzialek, D.; Lemaire, V.; Pisula, W.; Mullen, K.; Koldemir, U.; Reynolds,
42 J. R.; Lazzaroni, R.; Cornil, J.; Beljonne, D. High-Mobility Hole and Electron Transport
43 Conjugated Polymers: How Structure Defines Function. *Adv. Mater.* **2014**, *26*, 2119.
44
- 45 (36) Chen, M. S.; Niskala, J. R.; Unruh, D. A.; Chu, C. K.; Lee, O. P.; Fréchet, J. M. J.
46 Control of Polymer-Packing Orientation in Thin Films through Synthetic Tailoring of
47 Backbone Coplanarity. *Chem. Mater.* **2013**, *25*, 4088.
48
- 49 (37) Kim, K.-H.; Park, S.; Yu, H.; Kang, H.; Song, I.; Oh, J. H.; Kim, B. J. Determining
50 Optimal Crystallinity of Diketopyrrolopyrrole-Based Terpolymers for Highly Efficient
51 Polymer Solar Cells and Transistors. *Chem. Mater.* **2014**, *26*, 6963.
52
- 53 (38) Rand, B. P.; Cheyng, D.; Vasseur, K.; Giebink, N. C.; Mothy, S.; Yi, Y.; Coropceanu, V.;
54
55
56
57
58
59
60

1
2
3
4 Beljonne, D.; Cornil, J.; Bredas, J.-L.; Genoe, J. The Impact of Molecular Orientation on the
5 Photovoltaic Properties of a Phthalocyanine/Fullerene Heterojunction. *Adv. Funct. Mater.*
6 **2012**, *22*, 2987.

7
8 (39) Tumbleston, J. R.; Collins, B. A.; Yang, L.; Stuart, A. C.; Gann, E.; Ma, W.; You, W.;
9 Ade, H. The Influence of Molecular Orientation on Organic Bulk Heterojunction Solar Cells.
10 *Nat. Photon.* **2014**, *8*, 385.

11
12 (40) Jasieniak, J. J.; Seifert, J.; Jo, J.; Mates, T.; Heeger, A. J. A Solution-Processed MoO_x
13 Anode Interlayer for Use within Organic Photovoltaic Devices. *Adv. Funct. Mater.* **2012**, *22*,
14 2594.

15
16 (41) Kroger, M.; Hamwi, S.; Meyer, J.; Riedl, T.; Kowalsky, W.; Kahn, A. Role of the Deep-
17 Lying Electronic States of MoO₃ in the Enhancement of Hole-Injection in Organic Thin Films.
18 *Appl. Phys. Lett.* **2009**, *95*, 123301.

19
20 (42) Bartesaghi, D.; Perez, I. C.; Kniepert, J.; Roland, S.; Turbiez, M.; Neher, D.; Koster, L. J.
21 A. Competition Between Recombination and Extraction of Free Charges Determines the Fill
22 Factor of Organic Solar Cells. *Nat. Comm.* **2015**, *6*, 7083.

23
24 (43) Proctor, C. M.; Love, J. A.; Nguyen, T.-Q. Mobility Guidelines for High Fill Factor
25 Solution-Processed Small Molecule Solar Cells. *Adv. Mater.* **2014**, *26*, 5957.

26
27 (44) Kim, M.; Park, J. H.; Kim, J. H.; Sung, J. H.; Jo, S. B.; Jo, M.-H.; Cho, K. Lateral
28 Organic Solar Cells with Self-Assembled Semiconductor Nanowires. *Adv. Energy Mater.*
29 **2015**, *5*, 1401317.

30
31 (45) Li, W.; Albrecht, S.; Yang, L.; Roland, S.; Tumbleston, J. R.; McAfee, T.; Yan, L.; Kelly,
32 M. A.; Ade, H.; Neher, D.; You, W. Mobility-Controlled Performance of Thick Solar Cells
33 Based on Fluorinated Copolymers. *J. Am. Chem. Soc.* **2014**, *136*, 15566.

34
35 (46) Lampert, M. A. et al, Current Injection in Solids, *Academic Press*, New York, **1970**.

36
37 (47) Mihailetschi, V. D.; Koster, L. J. A.; Blom, P. W. M.; Melzer, C.; Boer, B.; Duren, J. K. J.;
38 Janssen, R. A. J. Compositional Dependence of the Performance of Poly(p-phenylene
39 vinylene): Methanofullerene Bulk-Heterojunction Solar Cells. *Adv. Funct. Mater.* **2005**, *15*,
40 795.

41
42 (48) Sim, M.; Shin, J.; Shim, C.; Kim, M.; Jo, S. B.; Kim, J. H.; Cho, K. Dependence of
43 Exciton Diffusion Length on Crystalline Order in Conjugated Polymers. *J. Phys. Chem. C*
44 **2014**, *118*, 760.

45
46 (49) Markov, D. E.; Amsterdam, E.; Blom, P. W. M.; Sieval, A. B.; Hummelen, J. C. Accurate
47 Measurement of the Exciton Diffusion Length in a Conjugated Polymer Using a
48 Heterostructure with a Side-Chain Cross-Linked Fullerene Layer. *J. Phys. Chem. A* **2005**, *109*,
49 5266.

50
51 (50) Kim, J. S.; Lee, Y.; Lee, J. H.; Park, J. H.; Kim, J. K.; Cho, K. High-Efficiency Organic
52 Solar Cells Based on End-Functional-Group-Modified Poly(3-hexylthiophene). *Adv. Mater.*
53 **2010**, *22*, 1355.

Figure Captions

Scheme 1. Synthetic route of monomers. *Reagents and conditions:* (a) NBS, chloroform/acetic acid, 2 h, RT, 82%; (b) AgF, Bis(benzonitrile)palladium (II) chloride, DMSO, 60 °C, 12 h, 78%; (c) Br₂, Fe, chloroform, RT, 2 h, 89% (d) n-BuLi, Et₂O, -5 °C, 2 h, HCl, 92%; (e) CuCN, DMF, 120 °C, 38 h, 95% (f) 1) NBS, chloroform, 50 °C, 10 h; 2) AgF, Bis(benzonitrile)palladium (II) chloride, DMSO, 60 °C, 7 h, 40%; (g) dodecyl methanesulfonate, Cs₂CO₃, DMF, microwave, 80 °C, 10 min, 73%; (h) DDQ, THF/dichloromethane, 50 °C, 12 h, 84%; (i) NBS, chloroform, 50 °C, 10 h, 91%; (j) AgF, Bis(benzonitrile)palladium (II) chloride, DMSO, 60 °C, 7 h, 55%.

Scheme 2. Synthetic route of new conjugated polymers.

Figure 1. (a) Normalized UV-vis absorption spectra of polymers in solution and thin films. (b) Energy level diagram of polymers.

Figure 2. Resonance structures of (a) PBDT-BT, (b) PBDT-BTC and (c) PBDT-BTCox.

Figure 3. Calculated optimized geometries and molecular orbitals for trimers of (a) PBDT-BT, (b) PBDT-BTC and (c) PBDT-BTCox (B3LYP/6-31G*).

Figure 4. (a) 2D GIXD patterns of the polymer thin films (top) neat polymers and (bottom) polymers/PC₇₁BM blend films. (b) The corresponding GIXD diffractogram profiles along the in-plane and out-of-plane directions.

Figure 5. (a) *J-V* curves of the BHJ solar cells based on PBDT-BT, PBDT-BTC and PBDT-BTCox under an illumination of AM 1.5G, 100 mA cm⁻². (b) EQE curves of BHJ solar cells.

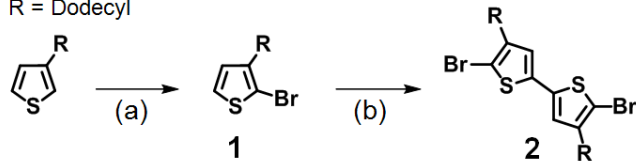
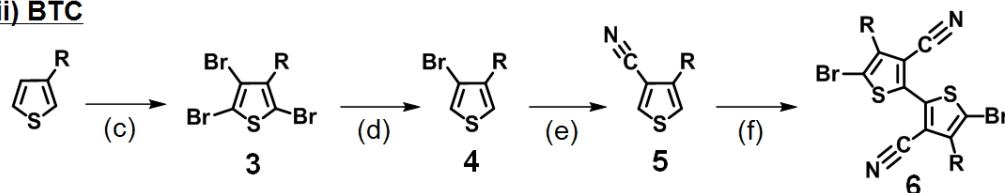
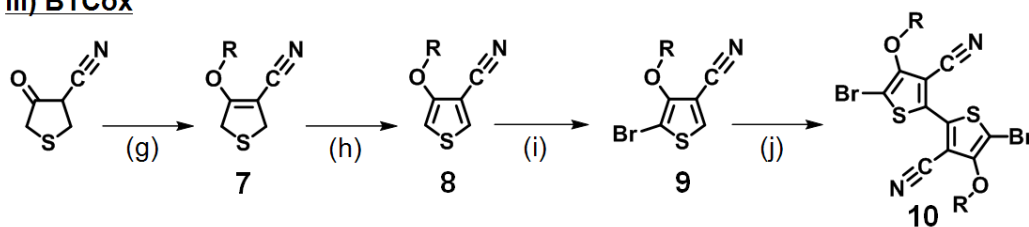
Figure 6. AFM topography of PBDT-BT/PC₇₁BM, PBDT-BTC/PC₇₁BM and PBDT-BTCox/PC₇₁BM without DIO (a, b, c) and with DIO (d, e, f). Scale bar = 500 nm.

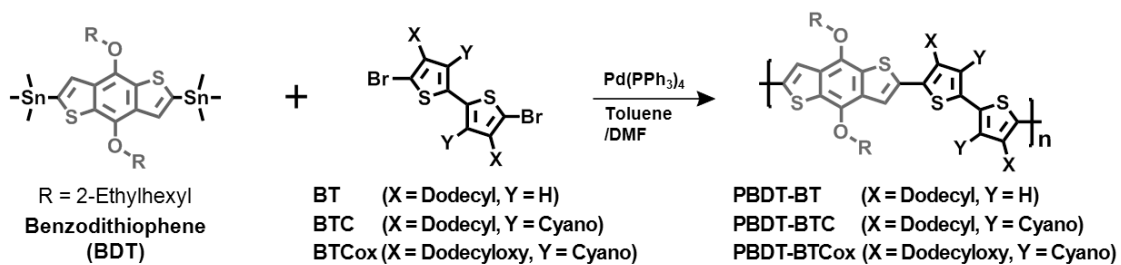
1
2
3
4 **Table 1.** Intrinsic properties of polymers
5
6

7 **Table 2.** Photovoltaic properties of polymers
8
9
10
11
12
13
14
15
16
17
18
19
20
21
22
23
24
25
26
27
28
29
30
31
32
33
34
35
36
37
38
39
40
41
42
43
44
45
46
47
48
49
50
51
52
53
54
55
56
57
58
59
60

i) BT

R = Dodecyl

**ii) BTC****iii) BTCox****Scheme 1**



Scheme 2

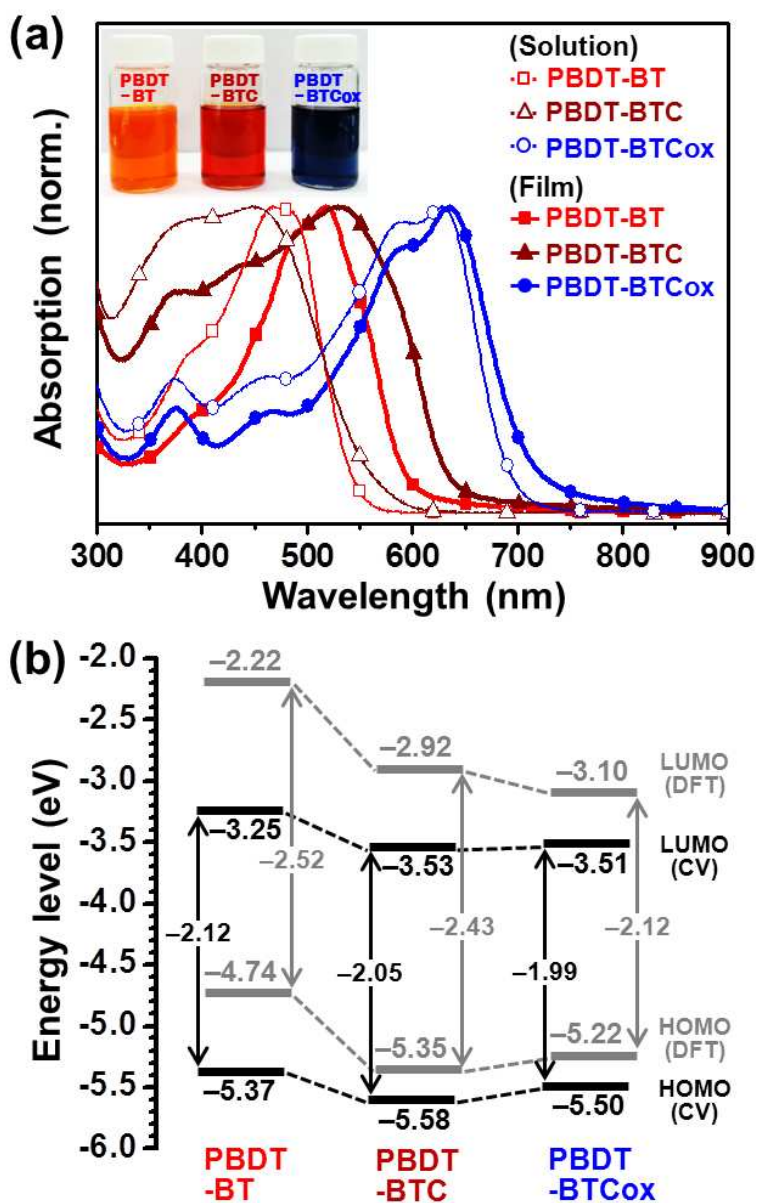
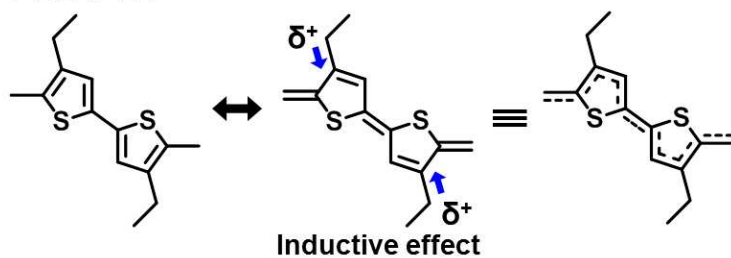
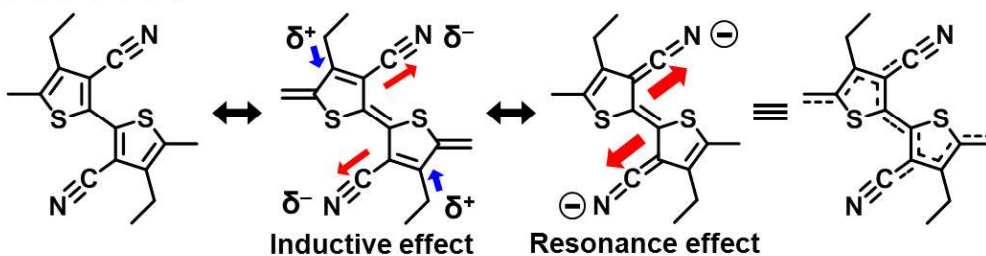
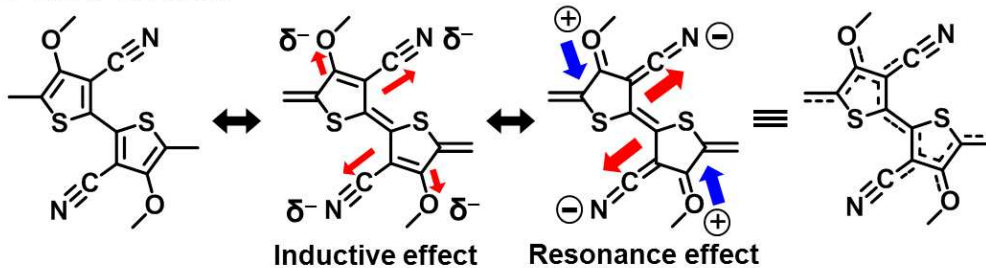


Figure 1

(a) PBDT-BT**(b) PBDT-BTC****(c) PBDT-BTCox****Figure 2**

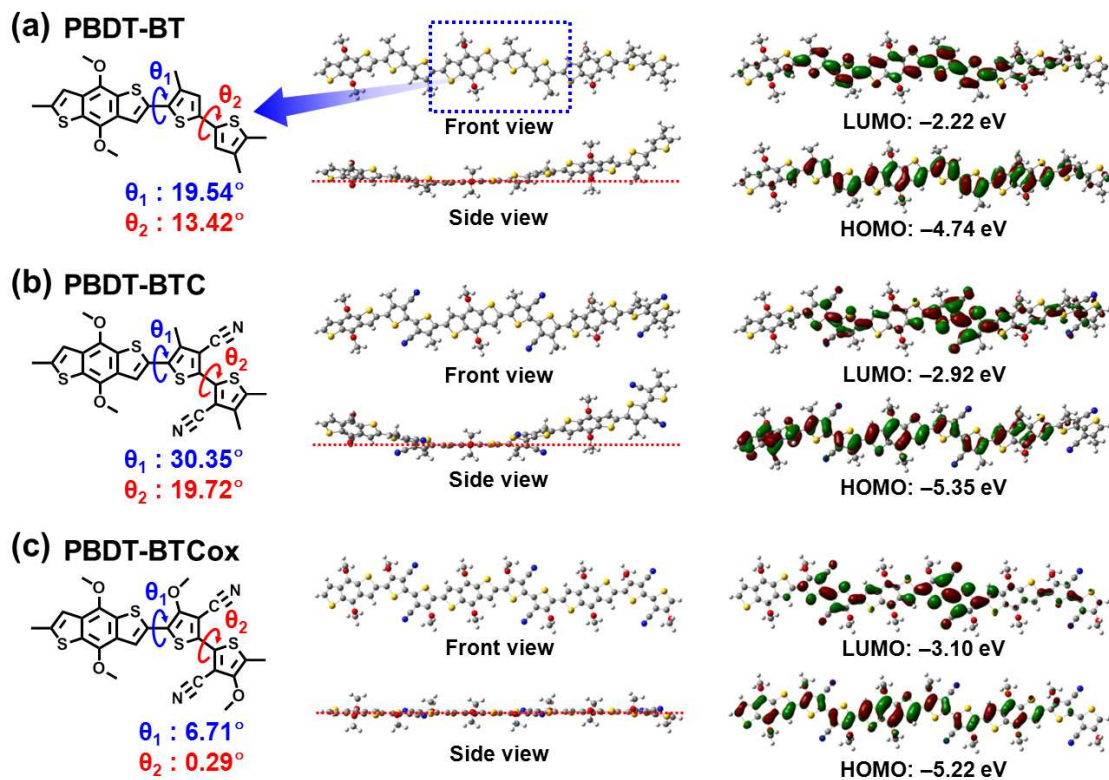


Figure 3

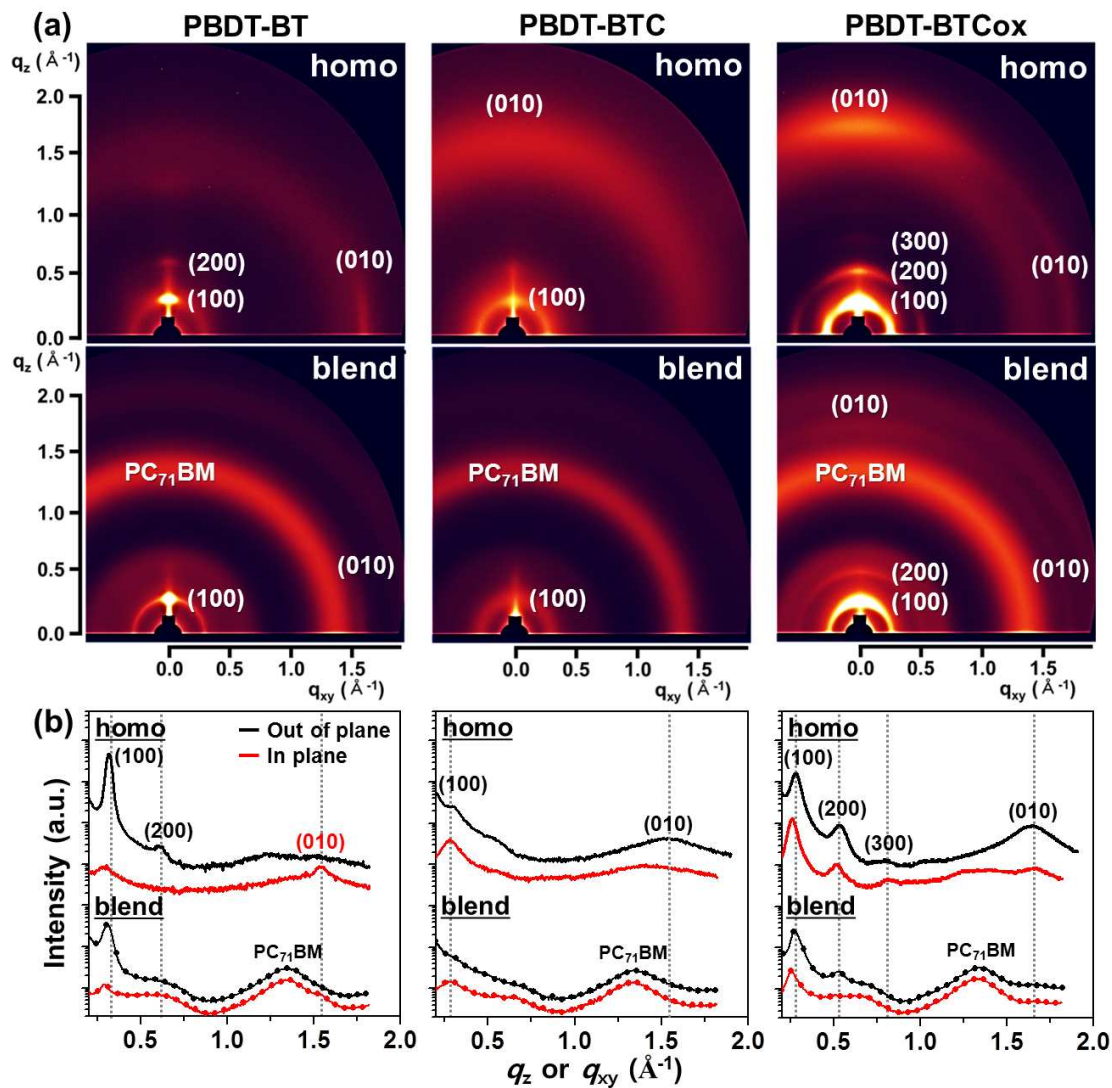


Figure 4

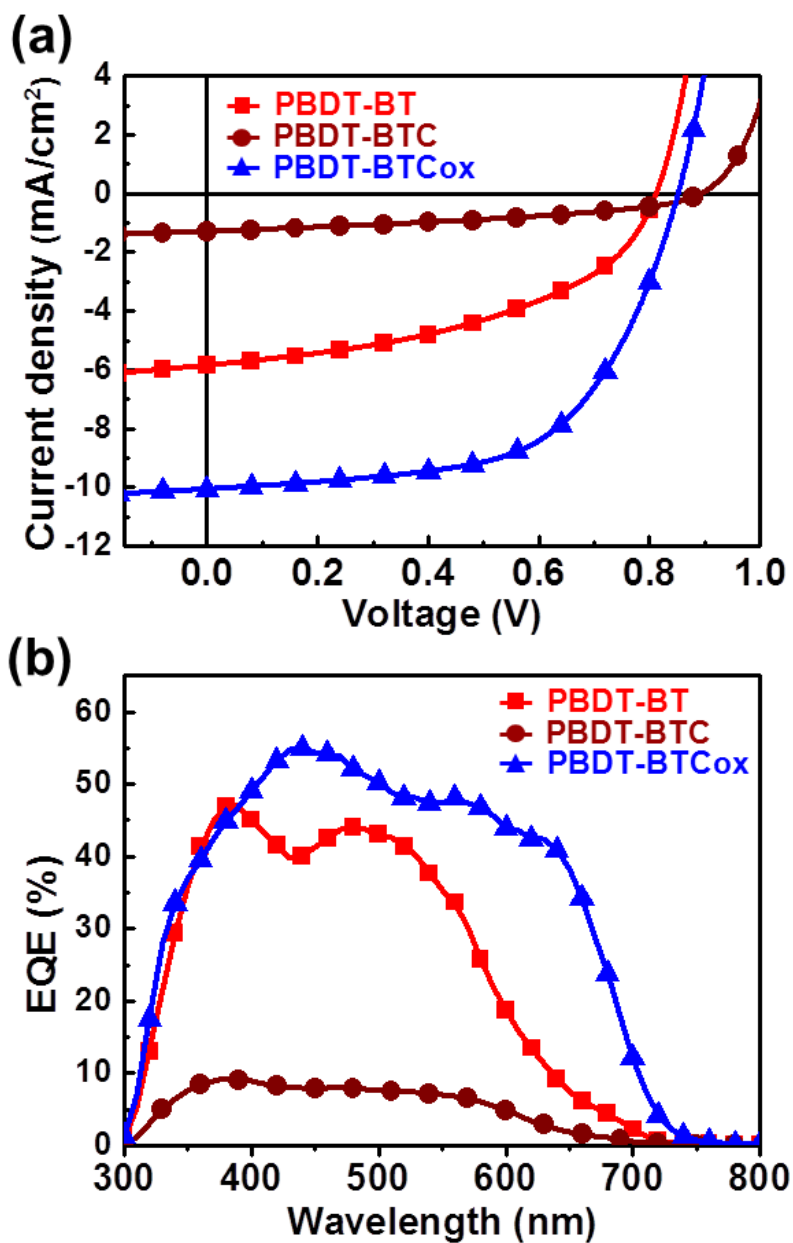


Figure 5

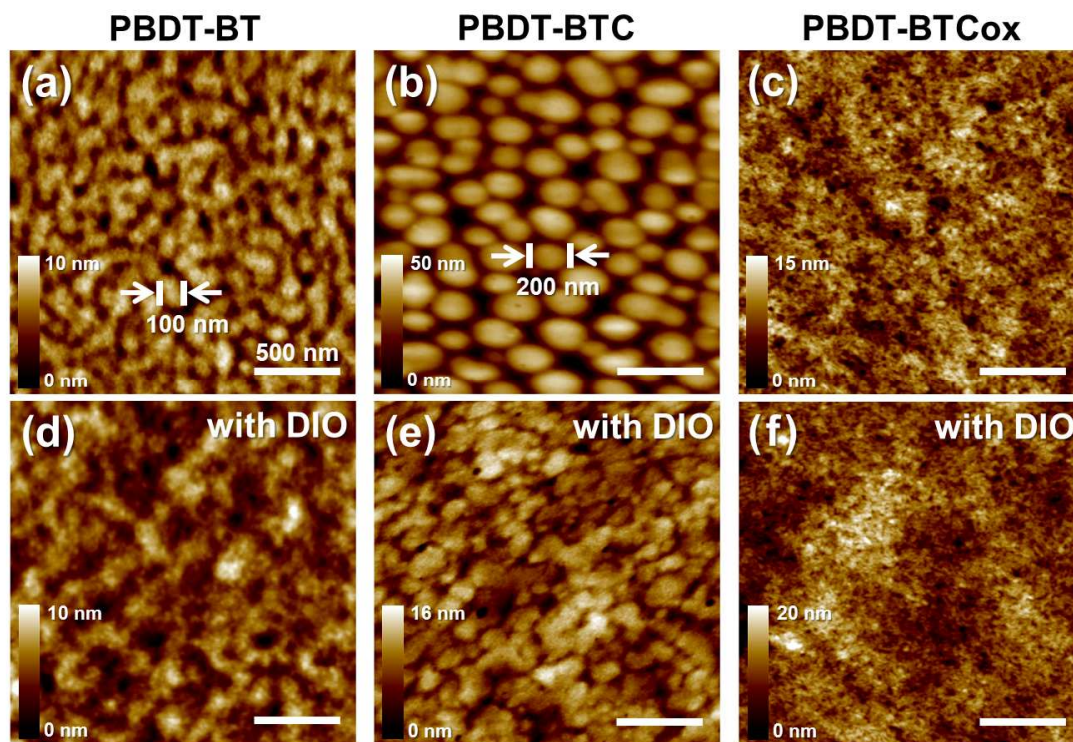


Figure 6

Table 1

Polymers	M_n (kDa) /PDI ^{a)}	T_d (°C)	$\lambda_{\max}^{\text{sol}}$ (nm)	$\lambda_{\max}^{\text{film}}$ (nm)	E_g^{opt} (eV) ^{b)}	HOMO (eV) ^{c)}	LUMO (eV) ^{c)}	E_g^{cv} (eV) ^{d)}
PBDT-BT	14.85/1.93	399	468	518	2.10	-5.37	-3.25	2.12
PBDT-BTC	11.82/3.37	389	448	529	1.96	-5.58	-3.53	2.05
PBDT-BTCox	37.59/1.77	401	629	635	1.74	-5.50	-3.51	1.99

^{a)} Determined by GPC using polystyrene standards in chlorobenzene as the eluent at 40 °C; ^{b)}

Estimated from the onset of the UV-vis spectrum; ^{c)} Onsets, potentials vs Fc/Fc⁺ ($E_{\text{HOMO}} = -$

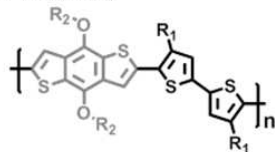
4.8 eV) as external reference; ^{d)} $E_g^{\text{cv}} = E_{\text{LUMO}} - E_{\text{HOMO}}$.

Table 2

Polymers	Solvent additive	Thickness (nm)	J_{sc} (mA cm ⁻²)	V_{oc} (V)	FF (%)	PCE_{max} (avg.) (%)
PBDT-BT	without	93 ± 4.3	5.86	0.82	45.8	2.20 (2.01)
	DIO 1.5v%	91 ± 4.0	1.70	0.89	46.4	0.77 (0.71)
PBDT-BTC	without	92 ± 4.3	1.30	0.90	40.0	0.48 (0.46)
	DIO 1.5v%	94 ± 6.0	1.27	0.98	41.4	0.55 (0.52)
PBDT-BTCox	without	111 ± 5.7	9.97	0.86	50.1	4.30 (4.27)
	DIO 1.5v%	114 ± 6.6	10.1	0.86	58.4	5.06 (4.90)

TOC graphic

- PBDT-BT



- PBDT-BTC



- PBDT-BTCox

